

Supplementary Information

Regulating Förster Resonance Energy Transfer and Cascade Energy Offset Achieves 19.6% Efficiency Ternary Organic Solar Cells

Jinghao Zhang, Anhai Liang,* Chaofeng Zhu, Silu Huang, Sein Chung, Hojun Ji, Jiyeong Shin, Kilwon Cho, Lijun Li,* Zhipeng Kan

Jinghao Zhang, Anhai Liang, Chaofeng Zhu, Silu Huang, Lijun Li, Zhipeng Kan

Center on Nanoenergy Research, Institute of Science and Technology for Carbon Peak & Neutrality, School of Physical Science & Technology, Guangxi University, Nanning 530004, China.

Sein Chung, Hojun Ji, Jiyeong Shin, Kilwon Cho

Department of Chemical Engineering, Pohang University of Science and Technology, Pohang 37673, South Korea.

Zhipeng Kan

State Key Laboratory of Featured Metal Materials and Life-cycle Safety for Composite Structures, Nanning, 530004 China

Corresponding Author

Anhai Liang - Center on Nanoenergy Research, Institute of Science and Technology for Carbon Peak & Neutrality, School of Physical Science & Technology, Guangxi University, Nanning 530004, China.

Email: 2207301067@st.gxu.edu.cn

Corresponding Author

Lijun Li - Center on Nanoenergy Research, Institute of Science and Technology for Carbon Peak & Neutrality, School of Physical Science & Technology, Guangxi University, Nanning 530004, China.

Email: lilijun@gxu.edu.cn

Experimental Materials.

D18-Cl, Y6, IDIC and PDIN were purchased from Organtec Ltd. PEDOT:PSS (CLEVIOSTM P VP AI 4083, Heraeus, Germany) was purchased from Xi'an Yuri Solar Co., Ltd. All materials were used as received without further purification.

Solar cell fabrication

Normal devices: Binary and ternary OSCs were prepared by ITO/PEDOT: PSS/ active layer /PDIN/Ag. The glass substrate was coated with indium tin oxide (ITO, device area: 0.0361 cm²). Ultrasonic cleaning of the substrate was performed in the order of dishwashing liquid, deionized water, acetone, deionized water and isopropyl alcohol for 15 minutes each. The ITO glass was then treated in an ultraviolet-ozone cleaner for 30 minutes. A layer of PEDOT:PSS (~30 nm) (CLEVIOSTM P VP AI 4083, Heraeus, Germany) was applied to the UV-treated ITO base by a static spin coating method, and the base is then transferred to the glove box for active layer deposition. All solutions were prepared with polymer donors (D18-Cl) and acceptors (Y6 and IDIC) in a nitrogen-filled glove box. Combine D18-Cl:IDIC、D18-Cl:Y6 and D18-Cl: Y6:IDIC (1:1.6, 14.3 mg/mL) were dissolved in chloroform (CF), heated and stirred on a magnetic stirrer for 2 hours, and the active layer solution was spin coated at 4000 rpm. Then PDIN solution (2.0 mg/mL in methanol with 0.3 vol% acetic acid) was spin-coated on the top of the active layer as the electron transport layer. The device is then placed in a high vacuum environment of 7×10^{-7} Torr, where Ag (100 nm) is thermally evaporated onto the active layer.

The inverted devices with laminated active layers: OSC devices were made using ITO-coated glass substrates. These substrates were cleaned with diluted detergent, deionized water, acetone and isopropyl alcohol in an ultrasonic bath, each for 10 min, and then treated for 30 min in a UV ozone chamber. Next, ZnO was spin-coated on ITO at 4500 rpm, heated at 150°C for 15 min, and moved to a N₂-filled glove box. PDMS was cut to match the glass slide size, attached to the slide, and soaked in isopropanol for 20 minutes. For the device structures with directly spin-coated D18-

Cl:Y6 and D18-Cl:Y6:IDIC, the structure is ITO/ZnO/PC₆₁BM/active layer/MoO₃/Ag. The active layer is dissolved in chloroform at a donor-acceptor ratio of 1:1.6, with a total concentration of 14.3 mg/ml. PC₆₁BM is dissolved in chloroform at 3 mg/ml. The solution is spin-coated onto PDMS (soaked for 20 minutes) at 3500 rpm for 30s. The PDMS is peeled off the glass slide and laminated onto the ZnO/PC₆₁BM layer. The active layer film adheres to the target substrate. Finally, 2nm MoO₃ and 100nm Ag are thermally deposited under 7×10^{-7} Pa vacuum.

UV-Vis Absorption.

UV-Vis absorption spectra of different blend films were recorded on a PerkinElmer LAMBDA 365 UV-Vis spectrophotometer.

Photoluminescence characterizations

The photoluminescence of the films was measured by a FLS1000 equipped with an integrating hemisphere at an excitation wavelength of 500 nm and 630 nm from Edinburgh Instruments Co., Ltd.

Photocurrent measurements

The J - V measurement was performed via a XES-50S1 (SAN-EI Electric Co., Ltd.) solar simulator (AAA grade) whose intensity was calibrated by a certified standard silicon solar cell (SRC-2020, Enlitech) under illumination of AM 1.5G 100 mW cm⁻². The AM 1.5G light source with a spectral mismatch factor of 1.01 was calibrated by the National Institute of Metrology. The intensity of the AM 1.5G spectra was calibrated by a certified standard silicon solar cell (SRC-2020, Enlitech) calibrated by the National Institute of Metrology. The J - V curves of small-area devices were measured in forwarding scan mode (from -0.2 V to 1.2 V) with a scan step length of 0.02 V.

SCLC Measurements

The carrier mobility (hole and electron mobility) of the photoactive layer was measured by fitting the dark current of the hole/electron diode with the space charge limited current (SCLC) model. The scan started from -5 V to 5 V. The measurements of pure electronic devices and pure hole devices are prepared. Electronic device structure of ITO/ZnO/BHJ/PDIN/Ag and only hole of ITO/PEDOT:PSS/BHJ/MoO3/Ag. The single-carrier device was connected to a Source Measure Unit (Keithley, Model 236 SMU) which provides DC voltage to the electron-only devices. The $J-V$ values of different DC voltages can be detected and recorded through SMU. The J-V characteristics were further analyzed by the space-charge-limited-current (SCLC) method to extract zero-field carrier mobilities, where SCLC is described by:

$$J = \frac{9\varepsilon_0\varepsilon_r\mu_0V^2}{8L^3} \exp\left[-(0.89\beta) \sqrt{\frac{V}{L}}\right]$$

where J is the current density, L is the film thickness of the active layer, μ_0 is the hole or electron mobility, ε_r is the relative dielectric constant of the transport medium, ε_0 is the permittivity of free space ($8.85 \times 10^{-12} \text{ F m}^{-1}$), $V (= V_{\text{appl}} - V_{\text{bi}})$ is the internal voltage in the device, where V_{appl} is the applied voltage to the device and V_{bi} is the built-in voltage due to the relative work function difference of the two electrodes.

Carrier extraction by linearly increasing voltage (CELIV)

According to the composite model of Mozer et al., the change of carrier density $n(t)$ with time can be expressed as:

$$n(t) = \frac{n_0}{1 + \left(\frac{t}{\tau_b}\right)^\gamma}$$

Where $n(t)$ is the charge density at time t , n_0 is the initial charge density, τ_b is the recombination lifetime, and γ is the dispersion parameter. γ closes to 1, indicating a nondispersive bimolecular recombination at room temperature. The closer γ is to 1, the fewer traps there are in the system, and the slower the rate of bimolecular recombination. In the dispersive bimolecular recombination, the decay of carrier density is given by:

$$\beta(t) = \frac{dn(t)/dt}{n^2(t)}$$

where $n(t)$ is the carrier density and $\beta(t)$ is dispersive bimolecular recombination rate at a delay time t . Substituting the first equation, the bimolecular recombination rate $\beta(t)$ can also be expressed as:

$$\beta(t) = \left(\frac{1}{\tau_b}\right) \gamma n_0^{-1} (t/\tau_b)^{\gamma-1}$$

The resulting $\beta(t)$ can be calculated from the fitting parameters n_0 , τ_b and γ using equation above.

Atomic Force Microscopy (AFM)

A Dimension Icon atomic force microscope (AFM) from Bruker was used to image the active layers in tapping mode. The glass substrate is exposed to ultraviolet ozone plasma for 15 minutes and spin coated directly in a nitrogen environment. The atomic force microscope is used for non-contact scanning, and the cantilever oscillates at a distance of 5 ~ 10 nm above the sample surface when detecting the sample surface.

By continuously changing the scale from 500 μm to 5 nm, the surface morphology of the film was observed, and finally the AFM image with the size of 2 x 2 μm was captured.

Transmission Electron Microscopy (TEM)

A layer of PEDOT: PSS is applied to the base, and then spin the film. The glass substrate was placed on the surface of deionized water, dissolved in water using the hydrophilicity of the PEDOT: PSS layer, then transferred to a 50-mesh copper grid on the substrate (China Electron Microscope), and corrected electron microscope (Titan ETEM G2 E-Twin) by spherical aberration observation at an accelerated operating voltage of 300 keV.

Grazing Incidence Wide-angle X-ray Scattering

Swept wide-angle X-ray scattering (GIWAXS), beamlines 3C SAXS-I and 9A U-SAXS were measured at the Pohang Light Source in South Korea. After careful selection, the incidence Angle is 0.12° to ensure that the X-ray completely penetrates the film. The e film is prepared according to the method described in the section on Device Fabrication. Using Scherrer equation to calculate coherence length (CCL) Peak $CCL = 2\pi k/\Delta q$, where k is a dimensionless shape factor (where $k = 0.9$) and Δq is the full half-peak width (FWHM) of a given peak.

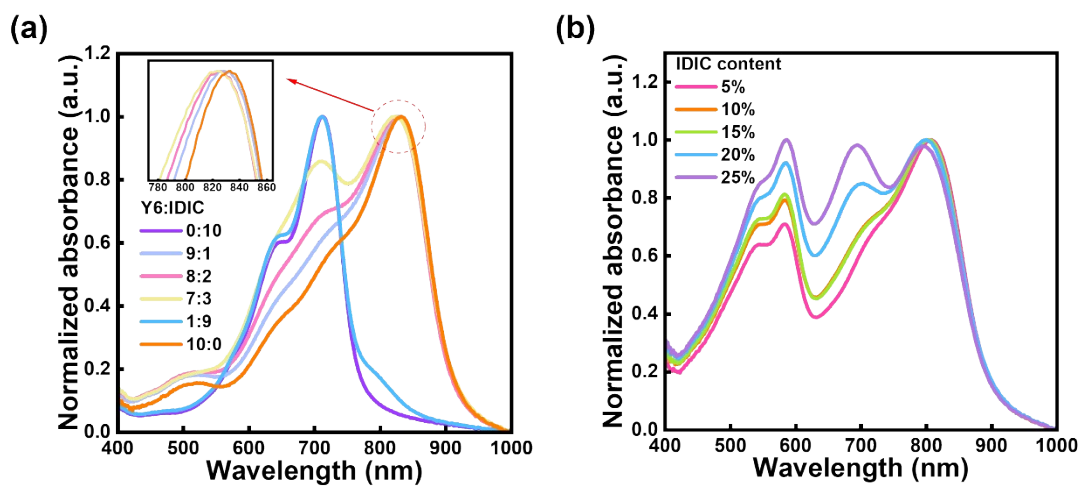


Figure S1. Normalized ultraviolet-visible absorption spectra: (a) Y6:IDIC with different ratios. (b) Ternary devices with varying IDIC contents.

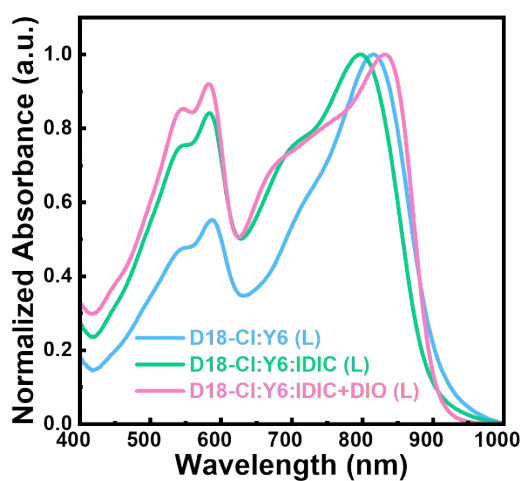


Figure S2. Normalized Absorbance of Blend Films.

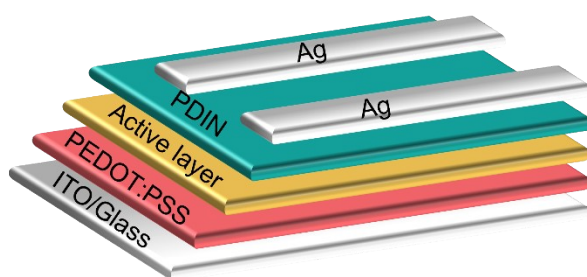


Figure S3. Schematic diagram of the structure of the transferred inverted device.

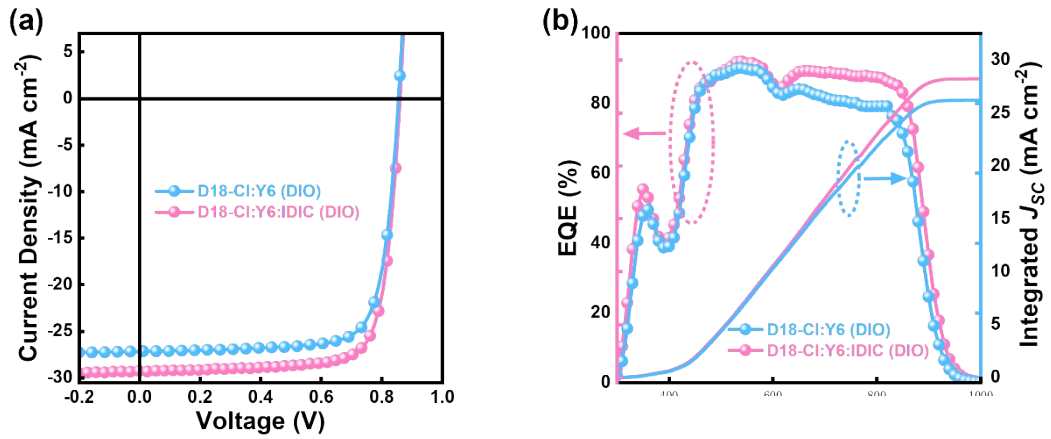


Figure S4. Optimized photovoltaic performance curves of D18-Cl:Y6 (DIO) and D18-Cl:Y6:IDIC (DIO): (a) Current-Voltage (J-V) characteristics. (b) External Quantum Efficiency (EQE).

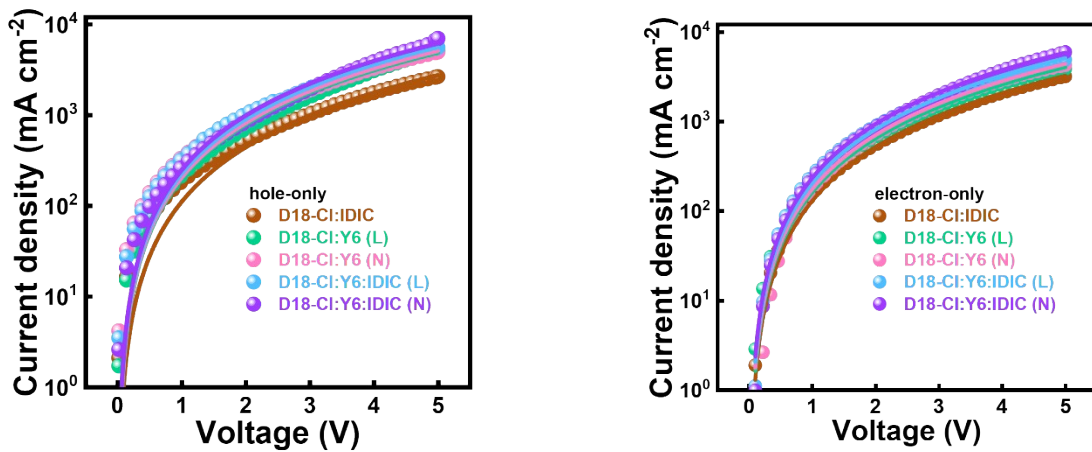


Figure S5. The hole and electron mobilities of the OSCs.

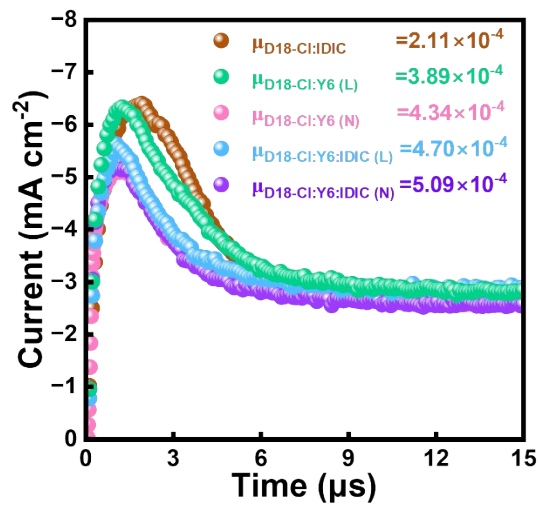


Figure S6. Photo-CELIV curves of the corresponding devices.

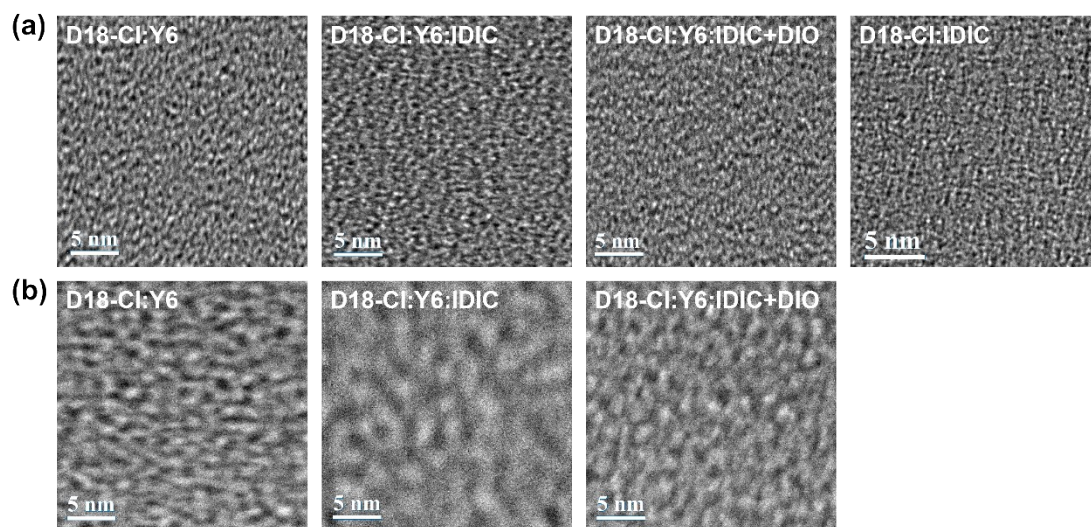


Figure S7: TEM images: (a) normal device; (b) the inverted devices with laminated active layers.

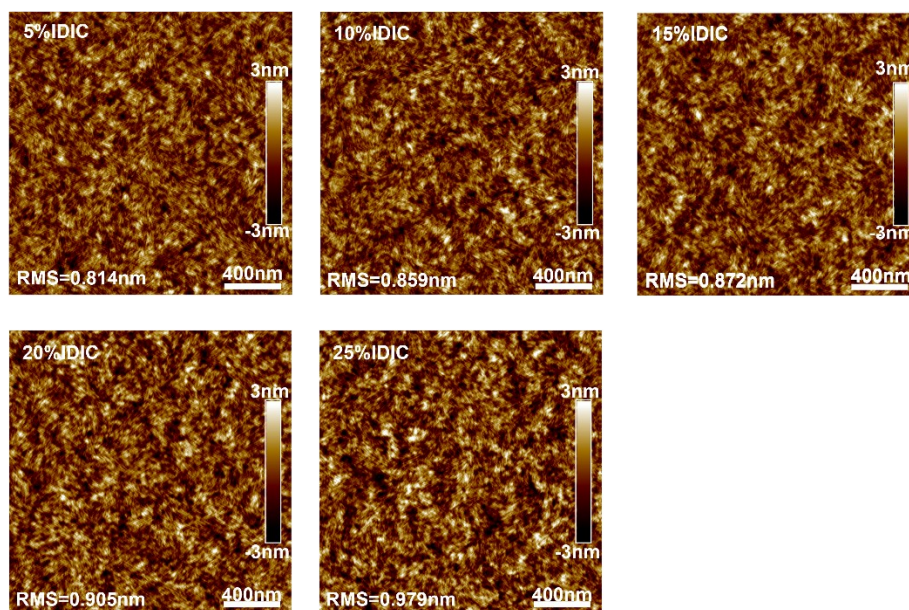


Figure S8. AFM images of IDIC at different ratios.

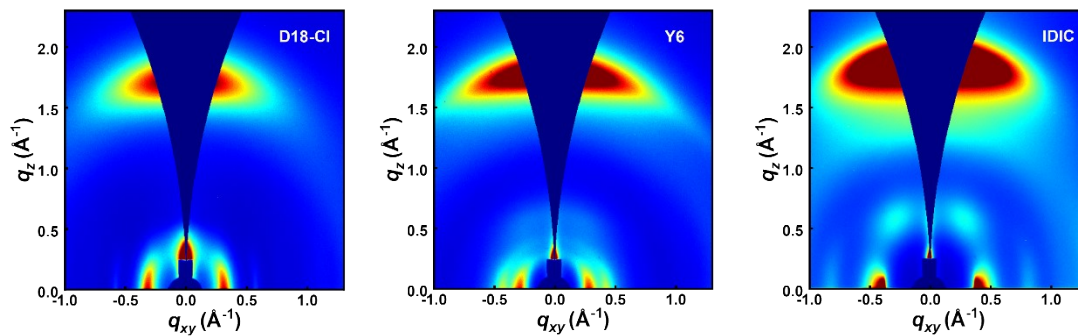


Figure S9. 2D GIWAXS patterns of the neat D18-Cl, Y6 and IDIC.

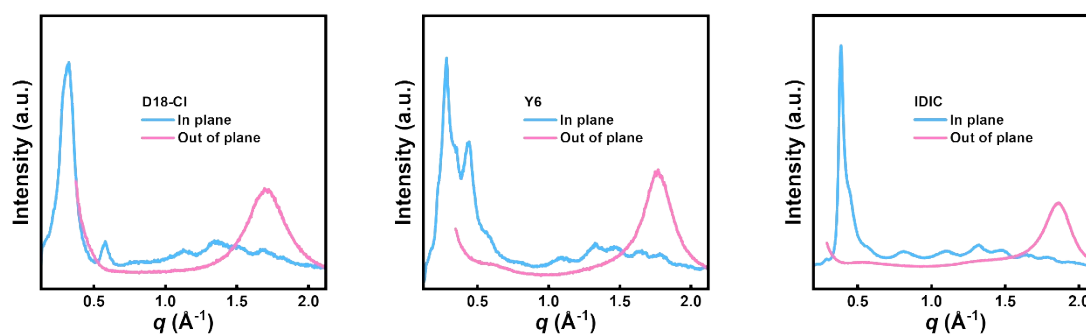


Figure S10. The in-plane (IP) and out-of-plane (OOP) line cuts of the neat D18-Cl, Y6 and IDIC.

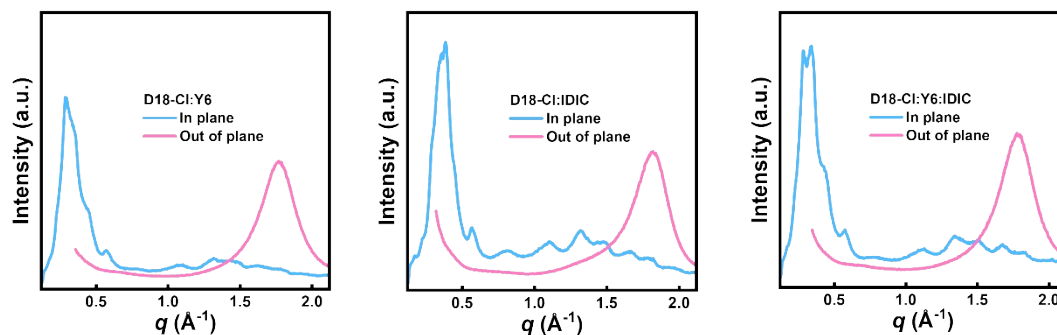


Figure S11. The in-plane and out-of-plane line cuts of the D18-Cl:Y6:IDIC ternary devices.

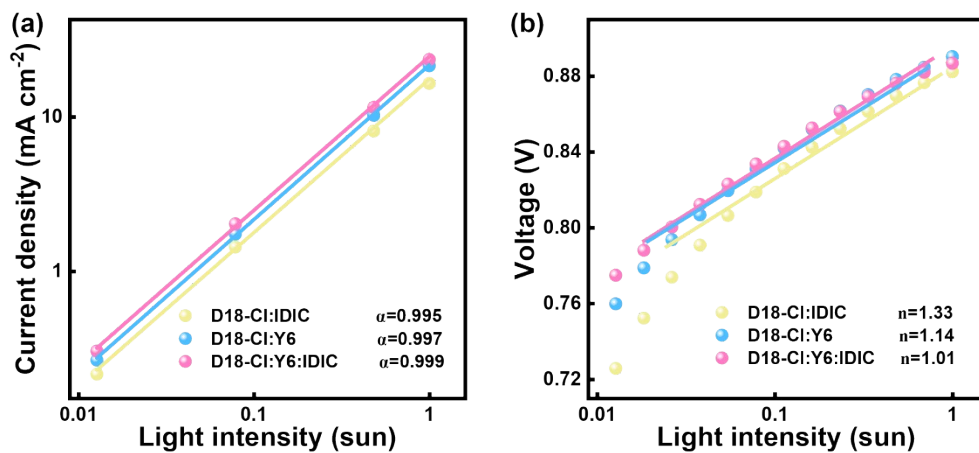


Figure S12. (a) J_{SC} and (b) V_{OC} dependence on the light intensity.

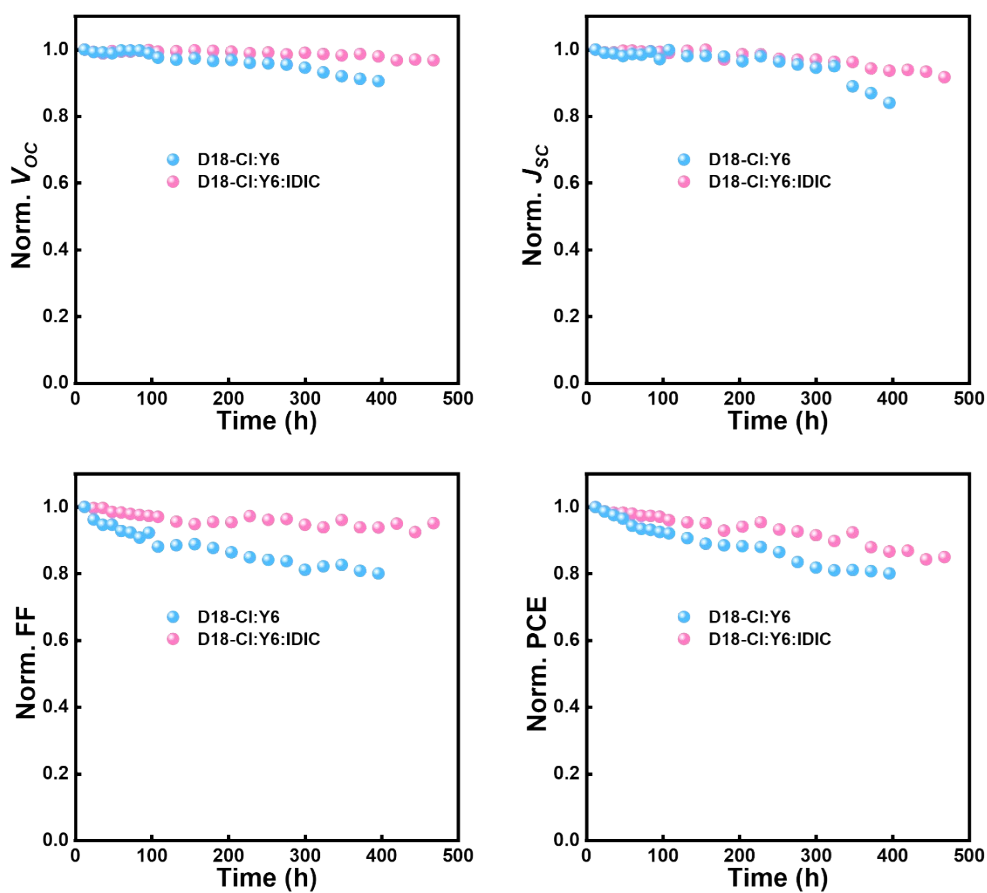


Figure S13. Stability of the device under indoor light exposure.

Table S1. Photovoltaic parameters of inverted binary D18-Cl:Y6 organic solar cells with different concentrations under 1.5G, 100 mW cm⁻² AM illumination.

Concentration	V_{OC} (V)	J_{SC} (mA cm ⁻²)	FF (%)	PCE (%)
14.3 mg/mL	0.874	26.10	67.17	15.33
12 mg/mL	0.875	26.65	65.38	15.24
10 mg/mL	0.861	25.49	64.38	14.13
8 mg/mL	0.848	18.98	57.56	9.27

Table S2. Photovoltaic parameters of the ternary OSCs with varied Y6: IDIC ratios under the illumination of AM 1.5G, 100 mW cm⁻².

Y6:IDIC	V_{OC} (V)	J_{SC} (mA cm ⁻²)	FF (%)	PCE (%)
1.52:0.08	0.877	27.64	74.78	18.13 (17.80±0.16)
1.44:0.16	0.880	27.79	75.98	18.59 (18.36±0.05)
1.36:0.24	0.889	27.60	74.20	18.22 (18.01±0.06)
1.28:0.32	0.894	27.54	72.65	17.89 (17.56±0.10)
1.2:0.4	0.896	27.18	71.85	17.50 (17.31±0.08)

Table S3. The J_{SC} from EQE spectra and the J_{SC} measured under AM1.5G simulated irradiance.

Photoactive layer	J_{SC} (mA cm ⁻²)	$J_{cal,EQE}$ (mA cm ⁻²)	Error (%)
D18-Cl:IDIC	16.17	15.37	4.9%
D18-Cl:Y6 (L)	26.10	25.50	2.3%
D18-Cl:Y6 (N)	26.93	26.15	2.9%
D18-Cl:Y6 ^a (N)	27.22	26.19	3.8%
D18-Cl:Y6IDIC (L)	27.92	26.79	4.0%
D18-Cl:Y6:IDIC (N)	27.79	27.25	1.9%
D18-Cl:Y6:IDIC ^a (N)	29.28	28.22	3.6%

a. With 0.5% (by volume) 1,8-diiodooctan

Table S4. The peak position and CCL in IP and OOP directions of neat D18-Cl, IDIC and Y6.

Component	Peak	Peak	d -spacing (Å)	FWHM (Å ⁻¹)	Crystalline Coherence
		position (Å ⁻¹)			Length ^a (Å)
D18-Cl	IP (100)	0.338	18.59	0.046	122.93
	OOP (010)	1.722	3.62	0.298	18.98
Y6	IP (100)	0.279	22.52	0.031	182.42
	OOP (010)	1.750	3.59	0.286	19.77
IDIC	IP (100)	0.388	16.19	0.032	176.71
	OOP (010)	1.860	3.37	0.194	29.15

^a Using Scherrer equation to calculate coherence length (CCL) Peak CCL = $2\pi k/\Delta q$, where k is a dimensionless shape factor (where $k = 0.9$) and Δq is the full half-peak width (FWHM) of a given peak.^[1,2]

Table S5. The peak position and CCL in IP directions of D18-Cl:IDIC、D18-Cl:Y6 and D18-Cl: Y6:IDIC.

Component	Peak	Peak position (\AA^{-1})	d -spacing (\AA)	FWHM (\AA^{-1})	Crystalline
					Coherence Length (\AA)
D18-Cl:IDIC	IP(010)	0.430	14.61	0.084	67.32
	IP(100)	0.349	18.00	0.095	59.52
D18-Cl:Y6	IP(010)	0.340	18.48	0.086	65.75
	IP(100)	0.286	21.97	0.050	113.10
D18-Cl:Y6:IDIC	IP(010)	0.354	17.75	0.043	131.51
	IP(100)	0.305	20.60	0.066	85.68

Table S6. The peak position and CCL in OOP directions of D18-Cl:IDIC、D18-Cl:Y6 and D18-Cl: Y6:IDIC.

Component	Peak	Peak position (\AA^{-1})	d -spacing (\AA)	FWHM (\AA^{-1})	Crystalline
					Coherence Length (\AA)
D18-Cl:IDIC	D18-Cl	1.842	3.41	0.181	31.24
	IDIC	1.734	3.62	0.239	23.66
D18-Cl:Y6	D18-Cl	1.796	3.50	0.179	31.59
	Y6	1.755	3.58	0.257	22.00
D18-Cl:Y6:IDIC	D18-Cl	1.810	3.47	0.174	32.50
	Y6:IDIC	1.766	3.56	0.249	22.71

Table S7. Detailed photovoltaic parameters of 20 devices (D18-Cl:Y6:IDIC(N) with 0.5% 1,8-diiodooctane).

V_{oc} (V)	J_{sc} (mA cm ⁻²)	FF (%)	PCE (%)
861	29.28	78.04	19.67
858	29.33	77.75	19.58
856	29.41	77.58	19.54
859	29.17	77.67	19.47
855	29.34	77.44	19.42
854	29.33	77.31	19.37
863	28.80	77.96	19.36
852	29.08	77.25	19.14
861	28.82	77.13	19.14
854	28.92	77.41	19.13
855	28.89	77.31	19.10
855	28.84	77.40	19.09
855	28.90	77.26	19.08
867	28.77	76.30	19.04
854	28.90	77.12	19.04
850	28.95	77.33	19.02
856	28.65	77.30	18.96
855	28.56	77.57	18.93
854	28.37	77.93	18.88
855	28.25	77.66	18.76

References

- [1] X. Wang, J. Wang, P. Wang, C. Han, F. Bi, J. Wang, N. Zheng, C. Sun, Y. Li, X. Bao. Embedded Host/Guest Alloy Aggregations Enable High-Performance Ternary Organic Photovoltaics. *Adv. Mater.*, **2023**, 35, 2305652.
- [2] Y. Sun, S. Chung, X. Huang, K. Cho, Z. Kan. Suppressing nongeminate recombination with two well-compatible polymer donors enables 16.6% efficiency all-polymer solar cells. *Chem. Eng. J.*, **2023**, 470, 144186.